ELSEVIER

Journal of Power Sources 86 (2000) 181–196

JOURNAL OF POWER SOURCES

www.elsevier.com/locate/jpowsour

Modelling of polymer electrolyte membrane fuel cells with variable degrees of water flooding

J.J. Baschuk, Xianguo Li *

Department of Mechanical Engineering, University of Waterloo, Waterloo, Ontario, Canada N2L 3G1

Accepted 13 October 1999

Abstract

Polymer electrolyte membrane (PEM) fuel cells have received increasing attention from both the public and fuel cell community due to their great potential for transport applications. The phenomenon of water flooding in the PEM fuel cells is not well understood, and few modelling studies have included the effect of water flooding. On the other hand, water management is one of the critical issues to be resolved in the design and operation of PEM fuel cells. In the present study, a mathematical model has been formulated for the performance and operation of a single polymer electrolyte membrane fuel cell. This model incorporates all the essential fundamental physical and electrochemical processes occurring in the membrane electrolyte, cathode catalyst layer, electrode backing and flow channel. A special feature of the model is that it includes the effect of variable degree of water flooding in the cathode catalyst layer and/or cathode electrode backing region on the cell performance. The model predictions have been compared with the existing experimental results available in the literature and excellent agreement has been demonstrated between the model results and the measured data for the cell polarisation curves. Hence, this model can be used for the optimisation of PEM fuel cell design and operation, and can serve as a building block for the modelling and understanding of PEM fuel cell stacks and systems.

Keywords: PEM fuel cells; Water flooding; Cathode catalyst layer

1. Introduction

Environmental concerns brought about by the use of fossil fuels have created a demand for non-polluting energy conversion and power generation technology. The polymer electrolyte membrane fuel cell (PEMFC) has shown promise as the leading candidate for use as a non-polluting power source. The PEMFC discharges water as waste, operates at low temperatures for quick start-up, and uses a solid polymer as an electrolyte which reduces both construction and safety complications.

The performance of a PEMFC can be illustrated by a voltage vs. current density plot, or polarisation curve. A polarisation curve for a single PEMFC is illustrated in Fig. 1. The polarisation curve can be divided into three regions characterised by activation overpotential, ohmic overpotential and concentration overpotential [1]. In the activation overpotential region, the dominant source of losses is due to resistance to electrochemical reactions. These losses, also referred to as activation losses, occur when slow electrochemical reactions are driven from equilibrium in order to produce electric current. As the current drawn increases, the activation losses also increase. In the ohmic overpotential region, activation losses increase at a slower rate than ohmic losses; losses from electronic and ionic resistance in the cell are the most significant source of performance degradation. In the concentration overpotential region, losses due to mass transport limitations are dominant. Concentration overpotential occurs when the chemical reaction is limited by the rate at which reactants can be supplied. This lack of reactants slows the electrochemical reaction, resulting in a lower cell potential.

It is the goal of the model developed here to model all three overpotential regions of a PEMFC in a unified, fundamental approach. An engineering model is used based on the previous work of Marr and Li [2,3]. The concentration overpotential region is dealt with by allowing liquid water to be present in the cathode catalyst layer and the cathode electrode backing; thus decreasing the concentra-

* Corresponding author.

0378-7753/00/$ - see front matter
PII: S0378-7753(99)00426-7

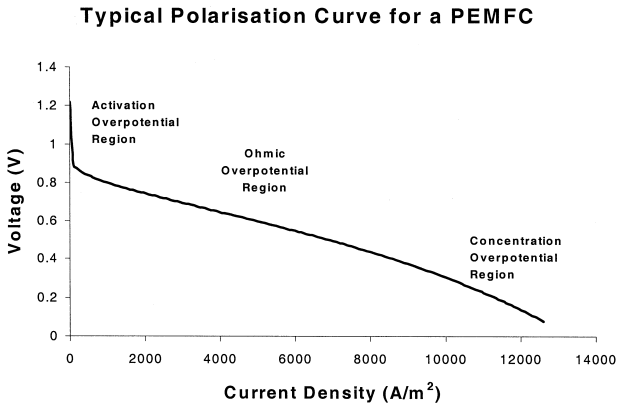

Fig. 1. Polarisation curve of a typical polymer electrolyte membrane fuel cell illustrating the activation, ohmic and concentration overpotential regions.

tion of oxygen for the cathode reaction. For single cells, the concentration overpotential region may be avoided in operation since it generally occurs at high current densities. However, for fuel cell stacks, operational experience indicates that water flooding can even occur at low current densities and may not be avoided for practical current densities. In fact, water management is one of the critical issues to be resolved in the design and operation of PEMFCs. Therefore, an effective model of PEMFC flooding is needed in order to properly model a PEMFC stack. It is expected that this model will further the understanding of the processes in a PEMFC and lead to improvements in performance.

There are presently several models for the performance of a single PEMFC. Kim et al. [4] developed a curve-fitting scheme based on experimental data that fits the entire polarisation curve of a PEMFC. Amphlett et al. [5,6] developed an empirical model for the Ballard Mark IV cell that combines performance losses into parametric equations based on cell operating conditions, such as pressure and operating temperature. It does not model the concentration overpotential region. Bernardi and Verbrugge [7,8] used an analytical approach. They developed a mathematical model of a PEMFC from fundamental transport properties where the losses incurred by the activation overpotential of the anode and cathode reactions, the ohmic losses incurred by the membrane and the ohmic losses due to the electrodes are subtracted from the reversible cell voltage. The membrane is assumed fully flooded and the void regions of the catalyst layer are assumed to contain membrane phase only. The model does not account for the concentration overpotential region of the polarisation curve. Springer et al. [9,10] also used an analytical approach where only the losses incurred by the cathode reaction and the membrane were considered. The membrane model allowed for variable hydration between the anode and cathode and thus variable ohmic resistance due to the hydration of the membrane. An empirical formula was used to relate the hydration of the membrane to the conductivity. The entire polarisation curve was modelled by incorporating flooding in the catalyst and backing layer. This was achieved by decreasing the porosity of the catalyst and backing layers, which increased the transport losses and the cathode overpotential. Weisbrod et al. [11] used the membrane model of Springer et al. [9,10] and added to it an activation overpotential term. They ignored diffusion through the membrane phase of the catalyst layer, assumed the catalyst layer was not flooded, and as a result, the concentration overpotential region of the polarisation curve was not modelled. The analytical models so far mentioned all assumed an isothermal, one-dimensional fuel cell. In contrast, Fuller and Newmann [12] investigated strategies for thermal and water management. Nguyen and White [13] developed a quasi two-dimensional model to account for heat and mass transport between the electrode and reactant gas mixture in the flow channel. Neither Ref. [12] nor Ref. [13] incorporated the possibility of reduced mass transfer due to water flooding. Bevers et al. [14] developed a dynamic simulation of the cathode with both heat and water balance. Reduced mass transport due to water flooding was incorporated by allowing the void fraction of the backing layer or catalyst layer to change according to the amount of liquid water present. Eikerling and Kornyshev [15] used approximations in order to find analytical solutions to the governing equations of the PEMFC for different regions in the cell polarisation curve. Their model does not incorporate the concentration overpotential region. Marr and Li [2,3] developed a simplified, engineering model of a PEMFC based on the catalyst layer of Weisbrod et al. [11] and the membrane model of Bernardi and Verbrugge [7,8]. As mentioned earlier, this is the model that will be used to incorporate the effect of water flooding on the PEMFC performance.

Therefore, the issue of flooding in a PEMFC, resulting in the concentration overpotential region, has not been fully examined in previous work. In the following sections, the formulation of the model will be presented. The model is then compared to experimental data available in the literature for model validation.

2. Model formulation

Before describing the formulation of this model, a brief description of the operation of a PEMFC will be given. A PEMFC converts the chemical energy of a fuel, such as hydrogen (H_2), and an oxidant, such as oxygen (O_2), into electrical energy. A schematic of a typical PEMFC is illustrated in Fig. 2. The basic theory of operation is as follows. On one side of the cell, referred to as the anode, fuel is supplied under pressure into the flow channels on the plate. The fuel for this model is humidified H_2 gas. The fuel diffuses through the porous electrode until it reaches the anode catalyst layer. At this layer, the hydro-

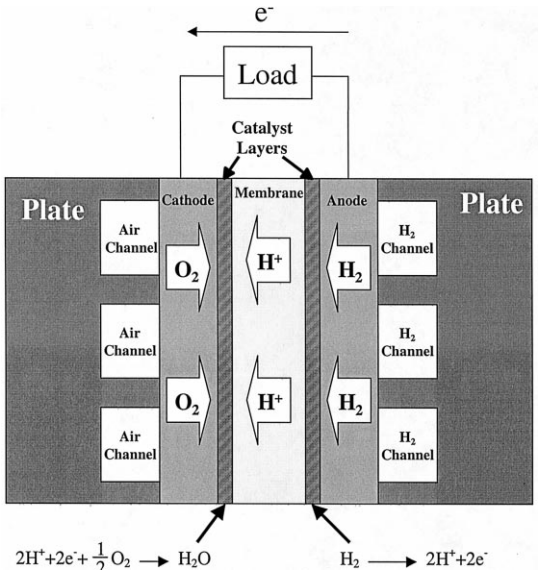

Fig. 2. Schematic of a polymer electrolyte membrane fuel cell.

gen reacts to form protons and electrons as shown in the reaction below:

$$H_2 \rightarrow 2H^+ + 2e^- \quad (1)$$

These protons are transferred through the membrane and to the cathode catalyst layer.

The other side of the PEMFC is referred to as the cathode. The oxidant flows in the plate channels and diffuses through the porous electrode until it reaches the cathode catalyst layer. The oxidant used in this model is humidified air or humidified O_2. Electrons from the electrode travel through either the platinum catalyst or catalysed carbon black particles to the catalyst surface, depending on the type of catalyst used. The oxygen is consumed along with the protons and electrons and the product, liquid water, is produced along with waste heat on the surface of the catalyst particles. The overall electrochemical reaction occurring at the reaction site may be represented by the reaction

$$2H^+ + 2e^- + \frac{1}{2}O_2 \rightarrow H_2O + \text{Heat} \quad (2)$$

The overall chemical reaction of the fuel cell is thus represented by the reaction

$$H_2 + \frac{1}{2}O_2 \rightarrow H_2O + \text{Heat} + \text{Electric Energy} \quad (3)$$

In the formulation of this model, the approach of Marr and Li [2,3] is used. The cell is assumed to operate under steady state conditions. A one-dimensional, isothermal approximation is used, since the cell thickness is small compared to its other dimensions. The membrane is assumed to be fully hydrated. This model differs from Marr and Li [2,3], however, by allowing liquid water as well as gas to be present in both the cathode catalyst layer and the cathode electrode or backing layer. Also, because the model of Marr and Li [2,3] found the overpotential due to the anode reaction to be negligible, the anode reaction overpotential is neglected in the present study.

As a result, the overall cell voltage (E) can be found by calculating the reversible cell voltage and subtracting the losses from it, as given below.

$$E = E_r - \eta_{act} - \eta_{ohmic,e} - \eta_{ohmic,p} - \eta_{ohmic,m} \quad (4)$$

In the above equation, E_r is the reversible cell voltage. The voltage loss due to resistance to the electrochemical reactions and mass transfer limitations in the cathode catalyst layer is denoted by η_{act}. The voltage loss due to the ohmic resistance of the electrodes, flow channel plate and membrane layer are denoted by $\eta_{ohmic,e}$, $\eta_{ohmic,p}$, and $\eta_{ohmic,m}$, respectively.

The following sections discuss the formulation of the reversible cell voltage, the voltage loss due to the ohmic resistance of the electrode and plates and the voltage loss due to the cathode catalyst layer reaction. The mass transfer of oxygen from the flow channel to the reaction sites at the cathode catalyst layer is also discussed, as it is instrumental in modelling the concentration overpotential region.

2.1. Reversible cell voltage

The reversible cell voltage (E_r) is the cell potential obtained at thermodynamic equilibrium. In this model, E_r is calculated from a modified version of the Nernst equation, with an extra term to account for changes in temperature from the standard reference temperature [1]. This is given by:

$$E_r = \frac{\Delta G}{2F} + \frac{\Delta S}{2F}(T - T_{ref}) + \frac{RT}{2F}\left[\ln(P_{H_2}) + \frac{1}{2}\ln(P_{O_2})\right] \quad (5)$$

where ΔG is the change in Gibbs free energy, F is the Faraday constant, ΔS is the change in entropy, R is the universal gas constant while P_{H_2} and P_{O_2} are the partial pressures (in atm) of hydrogen and oxygen, respectively. The variable T denotes the temperature of the cell, with T_{ref} denoting a reference temperature. Using standard values for ΔG, ΔS and T_{ref}, Eq. (5) can be simplified to [1]

$$E_r = 1.229 - 0.85 \times 10^{-3}(T - 298.15) + 4.31 \times 10^{-5} T\left[\ln(P_{H_2}) + \frac{1}{2}\ln(P_{O_2})\right] \quad (6)$$

2.2. Ohmic losses: electrode and plate

The ohmic voltage loss due to electrical resistance in the electrode and plate are modelled as an equivalent resistance, as shown in the schematic of Fig. 3. This model assumes that the current density is constant at the interface between the electrode and the catalyst layer and that the electrons take the shortest path to and from the reaction

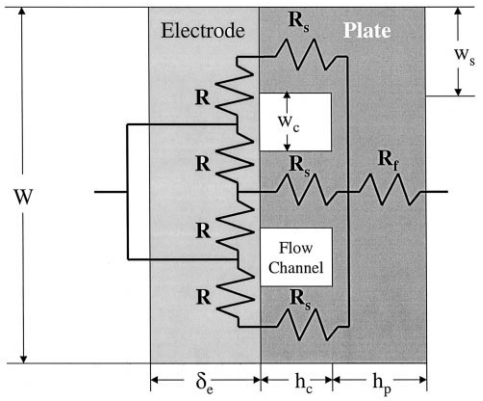

Fig. 3. The flow channel plate and electrode of a polymer electrolyte membrane fuel cell modelled as an equivalent electrical resistance.

sites. The total resistance for one electrode is found from the relation below [1]:

$$R_e = \frac{\rho_{R,e}^{eff}}{8 n_g \delta_e L}(w_c + w_s) \tag{7}$$

where w_c and w_s refer to the width of the flow channels and their corresponding supports while n_g is the number of flow channels in the cell. The width of the cell is denoted by W, the length by L and the thickness of the electrode is given the variable δ_c. The effective resistivity of the electrode, $\rho_{R,e}^{eff}$, can be derived from the bulk resistivity of the electrode ($\rho_{R,e}$) and the void fraction of the electrode (ϕ_e) by the Bruggeman's correction [1].

$$\rho_{R,e}^{eff} = \frac{\rho_{R,e}}{(1-\phi_e)^{3/2}} \tag{8}$$

The cathode and anode electrodes are assumed to be identical, hence the voltage loss due to the resistance of the electrode in a PEMFC becomes

$$\eta_{ohmic,e} = 2 R_e I_\delta WL \tag{9}$$

where I_δ denotes the cell current density.

Similarly, the equivalent resistance associated with the flow channel plate can be found. The equivalent resistance associated with the solid portion of the flow channel plates can be determined as follows:

$$R_f = \frac{\rho_{R,p} h_p}{WL} \tag{10}$$

where $\rho_{R,p}$ denotes the resistivity of the plate and h_p is the thickness of the solid portion of the plate. The resistance of the flow channel supports can be described by:

$$R_S = \frac{\rho_{R,p} h_c}{w_s L} \tag{11}$$

where h_c is the height of the flow channels and supports. Therefore, the total plate resistance can be determined by combining the two resistances to yield

$$R_p = \frac{\rho_{R,p}}{L}\left(\frac{h_p}{W} + \frac{h_c}{W - n_g w_c}\right) \tag{12}$$

The voltage loss due to the resistance of the plates in the PEMFC is

$$\eta_{ohmic,p} = 2 R_p I_\delta WL \tag{13}$$

2.3. Cathode catalyst layer

The cathode catalyst layer accounts for the majority of the voltage loss in a PEMFC cell. In modelling the cathode catalyst layer, the catalyst layer is assumed to be one-dimensional, isothermal and uniformly distributed. The void space within the catalyst layer is assumed large enough such that Knudsen diffusion is unimportant. The processes modelled in the catalyst layer are:

- The electrochemical reaction,
- Ohmic losses,
- Mass diffusion.

The rate of electrochemical reaction, assuming constant proton concentration, is given by the Butler–Volmer equation. The ohmic losses were found using Ohm's law. The mass diffusion was modelled using conservation of species and Fick's Law of diffusion. The governing differential equations for the catalyst layer can be expressed as follows [2]:

$$\frac{dI}{dz} = A_v i_{o,ref}\left(\frac{C}{C_{ref}}\right)^{\gamma}\left\{\exp\left(\frac{\alpha_c F \eta_{act}}{RT}\right) - \exp\left(-\frac{\alpha_a F \eta_{act}}{RT}\right)\right\} \tag{14}$$

$$\frac{dC}{dz} = \frac{I - I_\delta}{4FD_{O_2}^{eff}} \tag{15}$$

$$\frac{d\eta_{act}}{dz} = \left(\frac{1}{K_m^{eff}} + \frac{1}{K_s^{eff}}\right) I - \frac{I_\delta}{K_s^{eff}} \tag{16}$$

In the above equations, I denotes the protonic current density, C is the concentration of oxygen, η_{act} is the overpotential caused primarily by the resistance to the electrochemical reactions and due to finite rate of mass diffusion, I_δ is the cell current density and z is the distance into the catalyst layer, measured from the electrode/catalyst layer interface.

Eq. (14) describes the electrochemical reaction in the cathode catalyst layer. In this equation, $i_{o,ref}$ is the reference current density and is a function of cell temperature. It is an experimentally derived parameter and is given as a function of temperature for Nafion on platinum in Parthasarathy et al. [16]. The reaction order is denoted by γ and can be found analytically from the procedure in Newman [17], with a value of 0.5 resulting. The reference oxygen concentration, C_{ref}, is associated with $i_{o,ref}$ and in this model has a value of 12 mole/m^3. The cathodic and anodic transfer coefficients are denoted by α_c and α_a, which in this model have values of 1 and 0.5, respectively. The specific reaction surface is denoted by A_v and can be

Table 1
Catalyst surface area per unit mass of the catalyst (A_s) as a function of the amount of platinum catalyst on its carbon support as a mass or weight ratio (f_{Pt})

f_{Pt}	A_s (m^2/g)
0.1	140
0.2	112
0.3	88
0.4	72
0.6	32
0.8	11
1	28

derived from the catalyst mass loading per unit area of cathode (m_{Pt}), the catalyst surface area per unit mass of the catalyst (A_s) and the thickness of the catalyst layer (δ_c) [2] by the following.

$$A_v = \frac{m_{Pt} A_s}{\delta_c} \tag{17}$$

The catalyst surface area per unit mass of the catalyst is a function of the amount of platinum catalyst on its carbon support (f_{Pt}) as is illustrated in Table 1 [18].

Eq. (15) describes the mass transport through the cathode catalyst layer. The effective diffusion coefficient of oxygen in the catalyst layer is denoted by $D_{O_2}^{eff}$. The determination of this diffusion coefficient is discussed in Section 2.5.

Eq. (16) describes the ohmic losses through the catalyst layer. The effective conductivities of the membrane and the catalysed solids are denoted by K_m^{eff} and K_s^{eff}, respectively. These can be related to the bulk conductivity and corrected for the porosity of the catalyst layer as follows

$$K_m^{eff} = (l_m \phi_c)^{3/2} K_m \tag{18}$$

$$K_s^{eff} = (1 - \phi_c)^{3/2} K_s \tag{19}$$

where l_m denotes the fraction of membrane in the catalyst layer void region, ϕ_c is the void fraction of the catalyst layer and K_m and K_s are the bulk conductivities of the membrane and the solid catalyst. The void fraction of the catalyst layer can be calculated with the type and thickness of the catalyst layer as

$$\phi_c = 1 - \left(\frac{1}{\rho_{Pt}} + \frac{1 - f_{Pt}}{f_{Pt} \rho_c} \right) \frac{m_{Pt}}{\delta_c} \tag{20}$$

where ρ_{Pt} and ρ_c are the density of platinum and its carbon support, respectively, and f_{Pt} represents the amount of platinum catalyst on its carbon support (mass or weight ratio).

The value of K_m will depend on the membrane type and the temperature of the cell. For Nafion membrane, the electric conductivity is given by [7],

$$K_m = \frac{F^2 C_{H^+} D_{H^+}}{RT} \tag{21}$$

where C_{H^+} and D_{H^+} are the fixed-charge concentration and the apparent diffusion coefficient of H^+ in the membrane, respectively. However, the H^+ diffusion coefficient is also a function of temperature and viscosity of the pore fluid, μ_{H_2O}, which, in this model, is water. This is approximated by the relationship [17]

$$\frac{D_{H^+} \mu_{H_2O}}{T} = \frac{D_{H^+,\text{reference}} \mu_{H_2O,\text{reference}}}{T_{\text{reference}}} \tag{22}$$

The boundary conditions that apply to Eqs. (14)–(16) are that at the cathode electrode/catalyst layer interface, the protonic current density must be equal to zero because the electrode is ionically insulated. Also, at the other end of the catalyst layer, the protonic current density must be equal to the cell current density. Finally, the concentration profile of the oxygen must be continuous and as a result, the initial concentration of oxygen at the catalyst layer must be the same as that calculated for the electrode at that point. These boundary conditions are summarised below.

$$I(z = 0) = 0 \tag{23}$$

$$I(z = \delta_c) = I_\delta \tag{24}$$

$$C(z = 0) = C_{\text{catalyst}} \tag{25}$$

2.4. Ohmic losses: membrane

The membrane in this model is assumed to be fully hydrated and one-dimensional. As a result, the equation for the ohmic losses incurred by the membrane is [1].

$$\eta_{\text{ohmic,m}} = \delta_m \frac{\left(\frac{I_\delta}{K_m} + \frac{F K_P C_{H^+} \Delta P_{a\text{-}c}}{K_m \mu_{H_2O} \delta_m} \right)}{\left(1 + \frac{F^2 K_E C_{H^+}^2}{K_m \mu_{H_2O}} \right)} \tag{26}$$

In the above equation, δ_m denotes the thickness of the membrane, K_P is the hydraulic permeability, C_{H^+} is the fixed charge concentration, $\Delta P_{a\text{-}c}$ is the pressure differential across the membrane, K_E is the electrokinetic permeability, K_m is the electrical conductivity of the membrane and μ_{H_2O} is the viscosity of liquid water. As mentioned in Section 2.3, K_m is a function of cell temperature. The values for K_P, C_{H^+}, K_E and K_m for Nafion can be found in Bernardi and Verbrugge [7,8].

2.5. Oxygen transport

In this model, the mass transfer of oxygen from the flow channel to the reaction sites of the cathode catalyst layer will determine the shape of the polarisation curve in the concentration overpotential region. The oxygen in the flow channels must diffuse first to the surface of the electrode, then through the electrode to the catalyst layer surface as shown in Fig. 4. The flow from the channel to the electrode surface will be considered first.

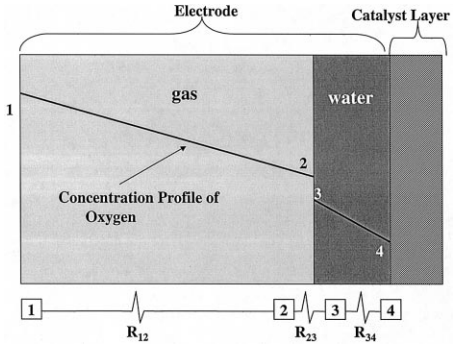

Fig. 4. Schematic of mass transport of oxygen in a partially flooded electrode.

The flow channel geometry is illustrated in Fig. 3. The area of the flow channels exposed to the electrode (A_c) can be related to the width of the flow channel supports (w_s), the width of the flow channel (w_c), the number of flow channels (n_g), the length of the cell (L) and the width of the cell (W) as follows

$$A_c = w_c\{n_g[L - (2w_s + w_c) + W]\} \quad (27)$$

Using an analogy between heat and mass transfer, the rate of oxygen transfer to the electrode surface due to convection from the flow channels can be calculated as

$$N_{O_2} = \frac{ShD_{O_2,bulk}A_c}{d_h}(C_{Channel} - C_{Surface}) \quad (28)$$

where N_{O_2} denotes the rate of oxygen transfer to the cell and is determined from

$$N_{O_2} = \frac{I_\delta WL}{4F} \quad (29)$$

In the above equations, the Sherwood number is denoted by *Sh* and, due to the laminar flow in the flow channels, is equal to 2.3. The hydraulic diameter of the flow channel is d_h while the diffusion coefficient of oxygen in the gas mixture of the flow channel is $D_{O_2,bulk}$. The concentration of oxygen in the flow channel is denoted by $C_{Channel}$ while the concentration of oxygen on the electrode surface is denoted by $C_{Surface}$. The concentration of oxygen in the flow channels and the surface are functions of distance along the flow channel. An average concentration on the surface of the electrode, C_1 in Fig. 4, was found by assuming a uniform flux of O_2 along the flow channel length (L_c) and then averaging $C_{Surface}$ over the flow channel length,

$$C_1 = \frac{1}{L_c}\int_0^{L_c} C_{surface}\,dl \quad (30)$$

where L_c is defined by

$$L_c = n_g[L - (2w_s + w_c)] + W \quad (31)$$

The bulk diffusion coefficient is calculated according to [19]:

$$D_{O_2,bulk} = \frac{1 - X_{O_2}}{\frac{X_{N_2}}{D_{O_2-N_2}} + \frac{X_{H_2O}}{D_{O_2-H_2O}}} \quad (32)$$

where X_{O_2}, X_{N_2} and X_{H_2O} are the average mole fractions of oxygen, nitrogen and water vapour in the flow channel, respectively. The binary diffusion coefficient of oxygen and nitrogen is denoted by $D_{O_2-N_2}$ and the binary diffusion coefficient of oxygen and water vapour is given the symbol $D_{O_2-H_2O}$. These binary diffusion coefficients are calculated using the Slattery–Bird equation [19].

The average mole fractions of the various constituents in the flow channel are calculated by taking the arithmetic average of the inlet and outlet mole fractions. In order to calculate these mole fractions, the variable for cell stoichiometry (s) must be introduced, which is defined as

$$s = \frac{N_{O_2,inlet}}{N_{O_2}} \quad (33)$$

where the rate of oxygen supplied at the flow channel inlet is denoted by $N_{O_2,inlet}$ while the stoichiometric rate of oxygen needed for the fuel cell operation (N_{O_2}) is calculated with Eq. (29).

It then follows that the mole fractions at the inlet and outlet of the cathode side flow channels can be calculated in terms of the stoichiometric rate and the stoichiometry of the cell, as given below:

$$N_{O_2,inlet} = sN_{O_2} \quad (34)$$

$$N_{N_2} = \frac{X_{N_2,inlet}}{X_{O_2,inlet}}N_{O_2,inlet} \quad (35)$$

$$N_{H_2O} = \frac{X_{H_2O}}{X_{N_2}}N_{O_2,inlet} \quad (36)$$

$$N_{O_2,outlet} = (s-1)N_{O_2} \quad (37)$$

$$X_{O_2,outlet} = \frac{N_{O_2,outlet}}{N_{O_2,outlet} + N_{N_2} + N_{H_2O}} \quad (38)$$

$$X_{N_2,outlet} = \frac{N_{N_2}}{N_{O_2,outlet} + N_{N_2} + N_{H_2O}} \quad (39)$$

$$X_{H_2O,outlet} = \frac{N_{H_2O}}{N_{O_2,outlet} + N_{N_2} + N_{H_2O}} \quad (40)$$

Note that in this model, the flow rate of water vapour and nitrogen is considered constant within the flow channel, because of the one-dimensional flow and steady state assumption.

The mole fractions at the inlet are set by the operating pressure of the cell and the composition of the cathode gas. The composition of air is taken as 21% O_2 and 79% N_2 and the mole fraction of water vapour is found by assuming the cathode gas has a relative humidity of 100%. The pressure used to calculate the mole fraction of the water vapour is the average pressure in the flow channel given by

$$P = P_{\text{inlet}} - \frac{1}{2}\Delta P \tag{41}$$

In the above, ΔP is found assuming laminar flow through a square passage using the equation below [1],

$$\Delta P = \frac{56.91\,\mu L_c v}{2\,d_h^2} \tag{42}$$

where v is the mass average velocity of the flow in the channels and μ is the viscosity of the gas mixture.

After diffusing to the surface, the oxygen must diffuse through the electrode before contacting the surface of the catalyst layer. The concentration at the surface of the catalyst layer can be found by examining the schematic of the oxygen profile shown in Fig. 4. If the rate of oxygen through the electrode is expressed as a flux, then the resistance to mass transfer shown in Fig. 4 can be expressed by a volume fraction divided by a diffusion coefficient written as

$$R_{12} = \frac{(1 - f_w)\,\delta_e}{D^{\text{eff}}_{O_2,\text{bulk}}} \tag{43}$$

$$R_{34} = \frac{f_w\,\delta_e}{D_{O_2 - H_2O_{(l)}}} \tag{44}$$

where $D^{\text{eff}}_{O_2,\text{bulk}}$ and $D^{\text{eff}}_{O_2-H_2O_{(l)}}$ are the effective diffusion coefficients of oxygen through the gas and liquid water. The variable f_w denotes the fraction of the void region in the electrode that is flooded by liquid water and it follows that $(1 - f_w)$ becomes the volume fraction of the gas mixture in the electrode. The effective diffusion coefficients can be expressed in terms of the void fraction of the electrode and the bulk diffusion coefficients as

$$D^{\text{eff}}_{O_2,\text{bulk}} = (\phi_e)^{3/2} D_{O_2,\text{bulk}} \tag{45}$$

$$D^{\text{eff}}_{O_2-H_2O_{(l)}} = (\phi_e)^{3/2} D_{O_2-H_2O_{(l)}} \tag{46}$$

The resistance R_{23} in Fig. 4 represents the resistance to mass transfer caused by the oxygen dissolving into the liquid water. The concentration at point 3 (C_3) can be related to the concentration at point 2 (C_2) by using the perfect gas law and Henry's law to relate partial pressure and concentration

$$C_3 = \frac{RT}{H_{O_2}} C_2 \tag{47}$$

where H_{O_2} is Henry's constant for oxygen gas dissolution in liquid water.

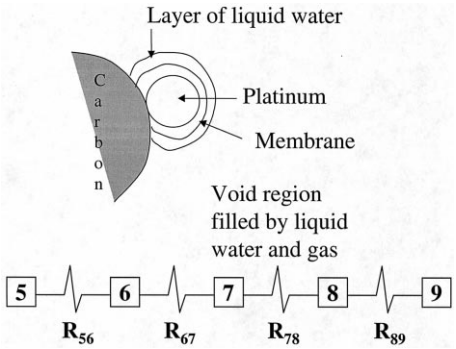

Fig. 5. Schematic of mass transport of oxygen in a partially flooded catalyst layer.

The concentration at point 4 (C_4) must be related to the concentration at point 1 (C_1). The concentration at point 1 can be related to the concentration at point 2 by using the resistance to mass transfer and the flux of oxygen through the electrode.

$$C_2 = C_1 - N''_{O_2} R_{12} \tag{48}$$

where N''_{O_2} is the molar flux of oxygen and is

$$N''_{O_2} = \frac{I_\delta}{4F} \tag{49}$$

Likewise, the concentration at point 3 can be related to that at point 4

$$C_3 = C_4 + N''_{O_2} R_{34} \tag{50}$$

Combining Eqs. (47), (48) and (50) yields

$$C_4 = C_1 \frac{RT}{H_{O_2}} - N''_{O_2}\left(\frac{RT}{H_{O_2}} R_{12} + R_{34}\right) \tag{51}$$

The binary diffusion coefficient of oxygen in liquid water is found using the Wilke–Chang equation [19] and Henry's constant in the units of atm cm^3/mole is calculated by the equation below [1].

$$\ln\left(H_{O_2}\right) = -\frac{666}{T} + 14.1 \tag{52}$$

The oxygen transport in the catalyst layer is formulated in the same approach as that of the electrode. The model of the catalyst layer allows the layer to be fully flooded, partially flooded or not flooded. A schematic of the catalyst layer when it is partially flooded is illustrated in Fig. 5. If the electrode is assumed not flooded and the catalyst layer is assumed partially flooded, then the resistance to mass transfer shown in Fig. 5 can be determined as

$$R_{56} = \frac{\left(1 - l_m - l_{H_2O}\right)\delta_c}{D^{\text{eff}}_{O_2,\text{gas},c}} \tag{53}$$

$$R_{78} = \frac{l_{H_2O}\,\delta_c}{D^{\text{eff}}_{O_2-H_2O_{(l)},c}} \tag{54}$$

$$R_{89} = \frac{l_m\,\delta_c}{D^{\text{eff}}_{O_2-m,c}} \tag{55}$$

In the equations above l_{H_2O} and l_m denote the volume fraction of liquid water and membrane, respectively, in the void region of the cathode catalyst layer. The resistance R_{56} represents the resistance to mass transfer associated with the gas mixture, R_{78} represents the resistance to mass transfer in the liquid water and R_{89} represents the resistance to mass transfer in the membrane. The effective diffusion coefficients of oxygen through the gas, water and membrane in the void region of the catalyst layer are denoted by $D^{eff}_{O_2-gas,c}$, $D^{eff}_{O_2-H_2O_{(l)}}$ and $D^{eff}_{O_2-m,c}$, respectively. These effective values are related to the bulk values by Bruggeman's correction

$$D^{eff}_{O_2-gas,c} = (\phi_c)^{3/2} D_{O_2,bulk} \quad (56)$$

$$D^{eff}_{O_2-H_2O_{(l)},c} = (\phi_c)^{3/2} D_{O_2-H_2O_{(l)}} \quad (57)$$

$$D^{eff}_{O_2-m,c} = (\phi_c)^{3/2} D_{O_2-m} \quad (58)$$

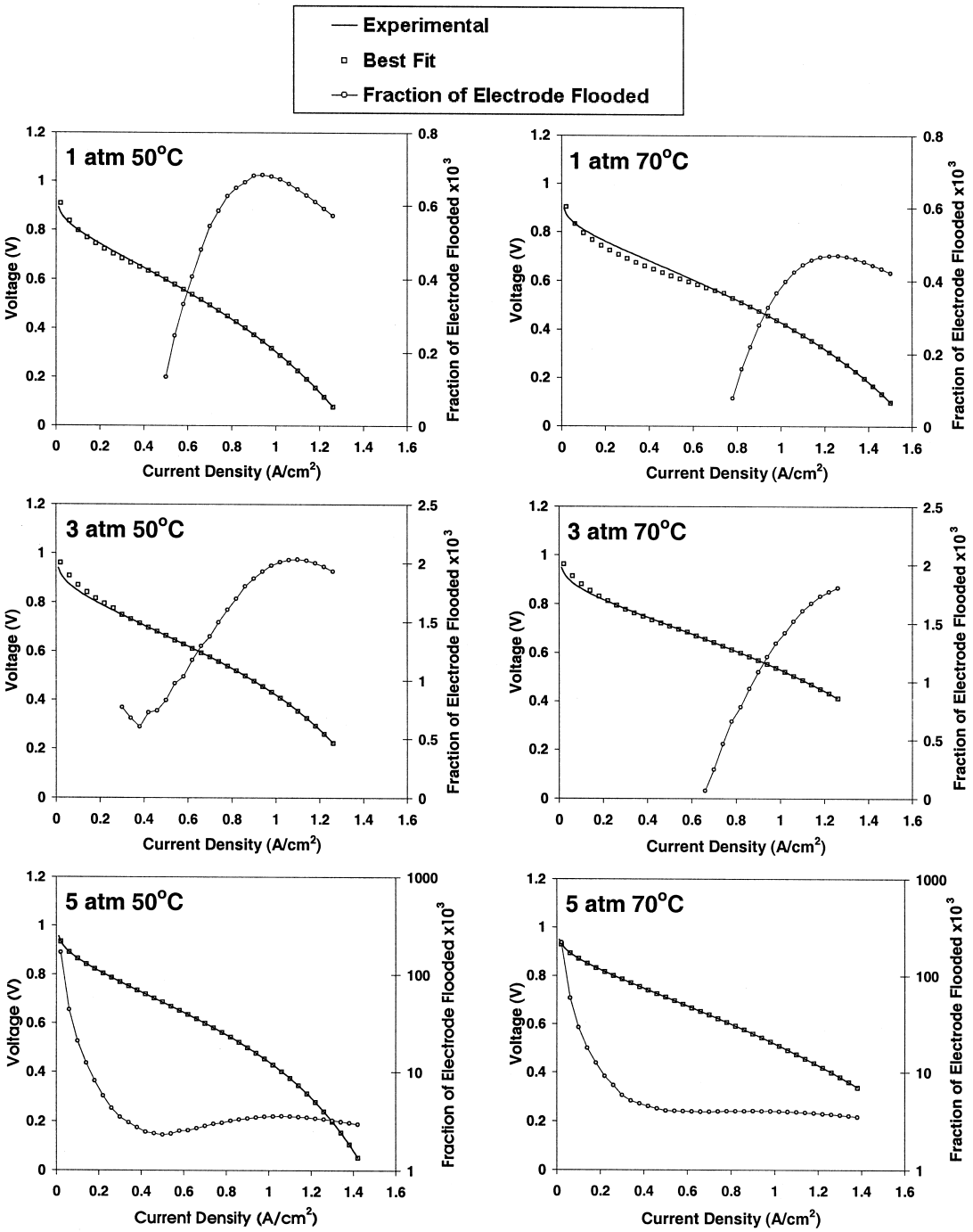

Fig. 6. Modelling the experimental data from Kim et al. [4] by incorporating different degrees of water flooding in the cathode electrode. Experimental data have oxygen as the cathode gas and hydrogen as the anode gas.

The diffusion coefficient of oxygen through the membrane is given by Ref. [1].

$$D_{O_2-m} = -1.0664 \times 10^{-5} + 9.0215 \times 10^{-6} \exp\left(\frac{T - 273.15}{106.65}\right) \quad (59)$$

The resistance R_{67} represents the resistance to mass transfer caused by oxygen dissolving in the liquid water and, as in the electrode mass transfer formulation, the concentration at point 6 (C_6) can be related to the concentration at point 7 (C_7) through the application of the perfect gas law and Henry's law

$$C_7 = C_6 \frac{RT}{H_{O_2}} \quad (60)$$

The concentration at point 6 (C_6) can be related to the concentration at point 5 (C_5) through the rate of oxygen and the resistance to mass transfer through the void region of the catalyst filled with gas by the following

$$C_6 = C_5 - N''_{O_2} R_{56} \quad (61)$$

Likewise, the concentration at point 9 can be related to that of point 7 with

$$C_9 = C_7 - N''_{O_2}(R_{78} + R_{89}) \quad (62)$$

Combining Eqs. (60)–(62) yields the relation

$$N_{O_2} = \frac{C_5\left(\frac{RT}{H_{O_2}}\right) - C_9}{\left(\frac{RT}{H_{O_2}}\right) R_{56} + R_{78} + R_{89}} \quad (63)$$

From the above equation, the equivalent diffusion coefficient for oxygen transport in the cathode catalyst layer, $D^{eff}_{O_2}$, used for the cathode catalyst layer Eq. (15) and the initial boundary condition (25) can be found. The equivalent diffusion coefficient can be written as

$$\frac{\delta_c}{D^{eff}_{O_2}} = \left(\frac{RT}{H_{O_2}} R_{56} + R_{78} + R_{89}\right) \quad (64)$$

Examining Eqs. (51) and (63), it is clear that $C_5(RT/H_{O_2})$ is equal to C_4. Thus, the initial concentration of oxygen at the electrode/catalyst layer interface, $C_{Catalyst}$, is equal to C_4.

3. Solution procedure

The procedure for solving the above formulation to yield a cell voltage for a given cell current and flooding parameters f_w and l_{H_2O} is as follows. First, the reversible cell voltage is calculated for a given cell temperature and

Table 2
Cell design parameters used to model the data from Kim et al. [4]

Parameter	Value
Resistivity of the anode and cathode electrode ($\rho_{R,e}$)	6×10^{-5} Ω m
Void fraction of the anode and cathode electrode (ϕ_e)	0.4
Thickness of the anode and cathode electrode (δ_e)	2.5×10^{-4} m
Width of the cell (W)	0.0707 m
Length of the cell (L)	0.0707 m
Width of the flow channels (w_c) of the anode and cathode	0.002 m
Width of the flow channel supports (w_s) of the anode and cathode	0.002 m
Number of flow channels (n_g) of the anode and cathode	12
Resistivity of the plate ($\rho_{R,p}$) of the anode and cathode	6×10^{-5} Ω m
Thickness of the solid plate (h_p) of the anode and cathode	0.002 m
Height of the flow channel (h_c) of the anode and cathode	0.002 m
Fraction of membrane in the void region of the cathode catalyst layer (l_m) when O_2 is used as the cathode gas	0.4
Fraction of membrane in the void region of the cathode catalyst layer (l_m) when air is used as the cathode gas	0.1
Catalyst mass loading per unit area of cathode (m_{Pt})	0.003 kg/m^2
Amount of platinum on carbon support in the cathode catalyst layer (f_{Pt}) when O_2 is used as the cathode gas	0.2
Amount of platinum on carbon support in the cathode catalyst layer (f_{Pt}) when air is used as the cathode gas	1
Catalyst layer thickness (δ_c) when O_2 is used as the cathode gas	1.23×10^{-5} m
Catalyst layer thickness (δ_c) when air is used as the cathode gas	2.57×10^{-7} m
Fixed-charge concentration in the membrane (C_{H^+})	1200 mole/m^3
Reference H^+ diffusion coefficient in the membrane ($D_{H^+,reference}$)	4.5×10^{-9} m^2/s^2
Thickness of the membrane (δ_m)	1.64×10^{-4} m
Hydraulic permeability of the membrane (K_P)	1.8×10^{-18} m^2
Electrokinetic permeability of the membrane (K_E)	7.18×10^{-20} m^2

pressure using Eq. (6). Next, the oxygen mass transport equations are solved in order to yield C_4 and $D_{O_2}^{eff}$. These values are needed to solve the catalyst layer equations. The catalyst layer equations are solved by combining Eqs. (14)–(16) to yield a single governing equation for the catalyst layer.

$$\frac{d^2C}{dz^2} = f\left(C, z, \eta_{act}|_{z=0}\right) \quad (65)$$

Eq. (65) was discretised using a quasi-linear approximation. Boundary conditions (23) and (24) were used to solve for the concentration profile through the catalyst layer while boundary condition (25) was used with a numerical approximation to solve for $\eta_{act}|_{z=0}$. This process yields η_{act}. After that, $\eta_{ohmic,e}$, $\eta_{ohmic,p}$ and $\eta_{ohmic,m}$ were solved for from Eqs. (9), (13) and (26), respectively. Therefore, with all the overpotentials known, the cell voltage can be calculated from Eq. (4).

4. Results and discussion

As mentioned in Section 1, the goal of this model is to predict the entire cell polarisation curve by introducing flooding in the cathode electrode backing and catalyst layer. The experimental data used for the validation of this

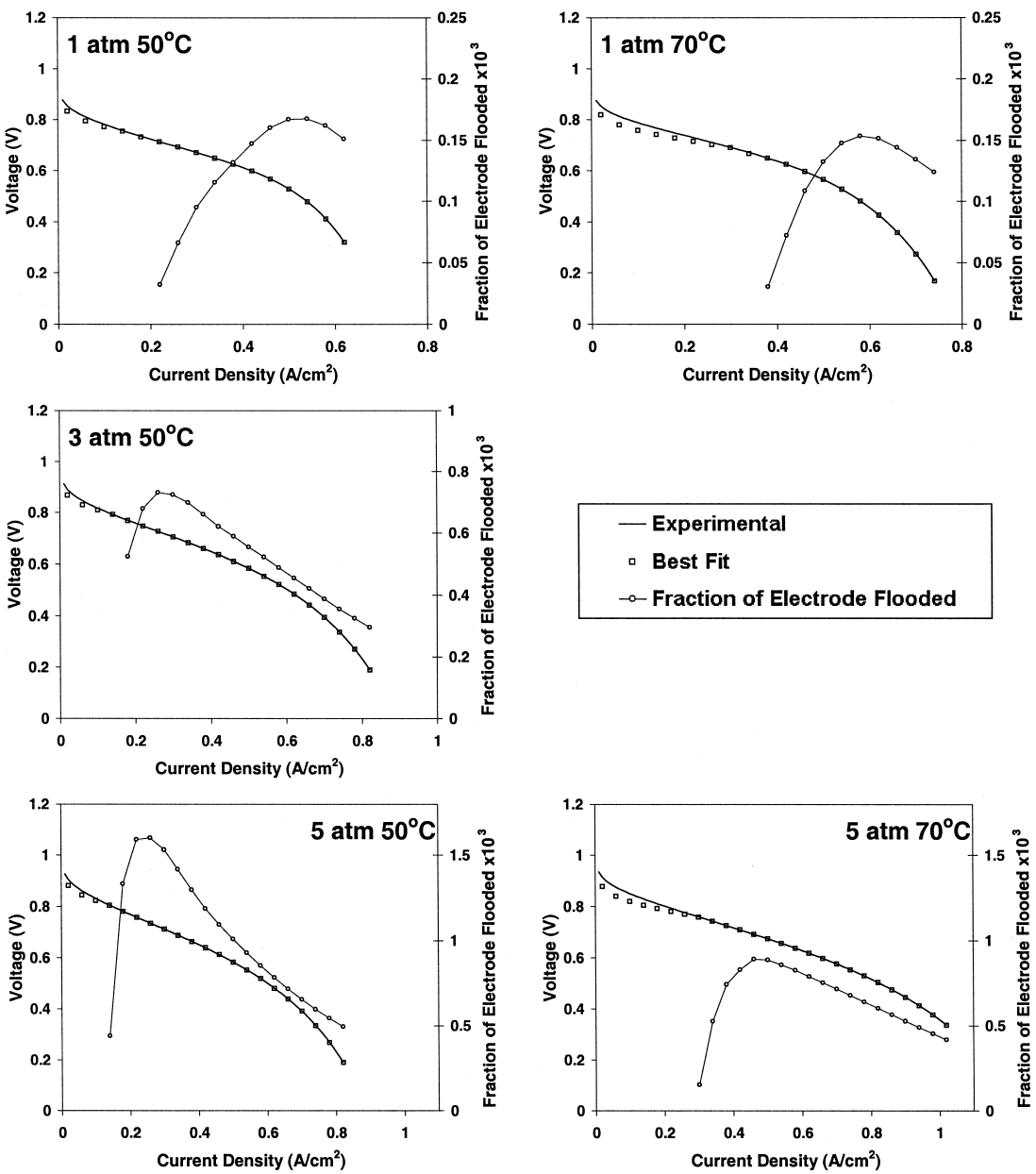

Fig. 7. Modelling the experimental data from Kim et al. [4] by incorporating different degrees of water flooding in the cathode electrode. Experimental data have air as the cathode gas and hydrogen as the anode gas.

model were from Kim et al. [4], Voss et al. [20] and Ledjeff-Hey and Heinzel [21]. In order to fit the polarisation curves presented, numerical values must be given for the parameters listed in the formulation. The parameters in this model can be classified into two categories: cell design parameters and cell operating parameters. Cell design parameters are values that are based on the physical structure of the PEMFC. Operating parameters are model parameters that will change depending on how the cell is being operated, such as pressure and temperature.

The first set of data fitted with this model is that of Kim et al. [4], in which the data were curve-fitted with an empirical equation for a PEMFC with oxygen or air as the oxidant and hydrogen as the fuel. The cell was operated with a cathode gas stoichiometry of 2 and at temperatures of 50°C and 70°C and pressures of 1, 3 and 5 atm, respectively. The result of applying the model to the data with oxygen as the oxidant is illustrated in Fig. 6. In order to match the experimental data of Kim et al. [4], the cell design parameters in the model were taken from the values listed in their paper, if given, or adjusted such that the model matched the experimental data at 1 atm and 50°C in the activation overpotential region of $I_\delta < 0.1$ A/cm^2. Once the cell design parameters were set in the model, the experimental data were modelled by varying the degree of flooding in the electrode backing and cathode catalyst layer until the model output voltage matched that of the experimental data. The cell design parameters used in the model are listed in Table 2. The figure shows that there is an excellent fit between the experimental data and the model when water flooding of the cathode electrode backing is incorporated. The effect of water flooding in the cathode catalyst layer on the cell voltage is small and, thus, is not illustrated in the figure. The minimal effect of flooding in the catalyst layer can be explained by the high resistance to mass diffusion caused by the membrane fraction in the void region of the catalyst layer. This resistance dominates the mass transfer in the catalyst region and thus the added resistance due to liquid water is negligible. The figure also illustrates that there are two distinctive flooding schedules. The first distinct flooding pattern is evident in the 1 and 3 atm pressure data and consists of a regimen in which the fraction of the electrode flooded increases with increasing current density until a maximum value is attained, after which the fraction of the water flooding decreases with increasing current density. The increasing portion of this flooding schedule can be explained by the increased water production at high current densities. After the fraction of the electrode flooded reaches a peak, the flooding decreases due to improved water removal by the higher volume flow rate of gas in the cathode flow channels. The second distinct flooding pattern is evident at a pressure of 5 atm. The cell is flooded at low current densities and the flooding decreases as the current density increases. In the 50°C data, the flooding then increases after it passes through a minimum, while for the 70°C data the flooding stabilises at an almost constant value of flooding. This behaviour can be explained by the cell being flooded initially and as the cell current density increases, the flow rate through the flow channels also increases and removes more water from the cathode; the fraction of the electrode flooded decreases. It can also be seen in the figure that an increase in cell temperature increases the current density at which flooding occurs in the 1 and 3 atm flooding schemes. Also, an increase in pressure corresponds with increased water flooding. It

Table 3
Cell design parameters used to model the data from Voss et al. [20]

Parameter	Value
Resistivity of the anode and cathode electrode ($\rho_{R,e}$)	6×10^{-5} Ω m
Void fraction of the anode and cathode electrode (ϕ_e)	0.4
Thickness of the anode and cathode electrode (δ_e)	2.5×10^{-4} m
Width of the cell (W)	0.1523 m
Length of the cell (L)	0.1523 m
Width of the flow channels (w_c) of the anode and cathode	0.003 m
Width of the flow channel supports (w_s) of the anode and cathode	0.003 m
Number of flow channels (n_g) of the anode and cathode	24
Resistivity of the plate ($\rho_{R,p}$) of the anode and cathode	6×10^{-5} Ω m
Thickness of the solid plate (h_p) of the anode and cathode	0.003 m
Height of the flow channel (h_c) of the anode and cathode	0.003 m
Fraction of membrane in the void region of the cathode catalyst layer (l_m)	0.15
Catalyst mass loading per unit area of cathode (m_{Pt})	0.04 kg/m^2
Amount of platinum on carbon support in the cathode catalyst layer (f_{Pt})	1
Catalyst layer thickness (δ_c)	4.65×10^{-6} m
Fixed-charge concentration in the membrane (C_{H^+})	1200 mole/m^3
Reference H^+ diffusion coefficient in the membrane ($D_{H^+,reference}$)	4.5×10^{-9} m^2/s^2
Thickness of the membrane (δ_m)	2.20×10^{-4} m
Hydraulic permeability of the membrane (K_P)	1.8×10^{-18} m^2
Electrokinetic permeability of the membrane (K_E)	7.18×10^{-20} m^2

Table 4
Cell design parameters used to model the data from Ledjeff-Hey and Heinzel [21]

Parameter	Value
Resistivity of the anode and cathode electrode ($\rho_{R,e}$)	6×10^{-5} Ω m
Void fraction of the anode and cathode electrode (ϕ_e)	0.4
Thickness of the anode and cathode electrode (δ_e)	2.5×10^{-4} m
Width of the cell (W)	0.0707 m
Length of the cell (L)	0.0707 m
Width of the flow channels (w_c) of the anode and cathode	0.002 m
Width of the flow channel supports (w_s) of the anode and cathode	0.002 m
Number of flow channels (n_g) of the anode and cathode	12
Resistivity of the plate ($\rho_{R,p}$) of the anode and cathode	6×10^{-5} Ω m
Thickness of the solid plate (h_p) of the anode and cathode	0.002 m
Height of the flow channel (h_c) of the anode and cathode	0.002 m
Fraction of membrane in the void region of the cathode catalyst layer (l_m)	1
Catalyst mass loading per unit area of cathode (m_{Pt})	0.04 kg/m^2
Amount of platinum on carbon support in the cathode catalyst layer (f_{Pt})	1
Catalyst layer thickness (δ_c)	2.19×10^{-6} m
Fixed-charge concentration in the membrane (C_{H^+})	1200 mole/m^3
Reference H^+ diffusion coefficient in the membrane ($D_{H^+,reference}$)	4.5×10^{-9} m^2/s^2
Thickness of the membrane (δ_m)	2.20×10^{-4} m
Hydraulic permeability of the membrane (K_P)	1.8×10^{-18} m^2
Electrokinetic permeability of the membrane (K_E)	7.18×10^{-20} m^2

should also be noted that the fraction of electrode flooded is small and as a result, a small amount of water present in the electrode backing can severely influence performance at high current densities.

The data from Kim et al. [4] using air as the oxidant was also modelled and the result is illustrated in Fig. 7. The data from a pressure of 3 atm and a temperature of 70°C was not modelled because of a discrepancy between the empirical curve and the plotted curve in Kim et al. [4]. Ideally, one set of cell design parameters should have been capable of modelling all of the experimental data, however different cell design parameters were needed for the oxygen and air data because the model under-estimated the cell voltage if the cell design parameters used for the oxygen data were used to model the air data of Kim et al. [4]. One possible explanation for this discrepancy could be that different cells were used to gather the oxygen and air data in Kim et al. [4]. Another explanation is that contamination in the gas streams influenced the data collected by Kim et al. [4]. Also, it is possible that a two or three-dimensional phenomenon is responsible for this discrepancy, which is not included in the one-dimensional model presented here. Using different cell design parameters, a good fit between the model and experimental data resulted. The cell design parameters used to model the experimental air data are listed in Table 2. Unlike the oxygen data of Fig. 6, Fig. 7 illustrates only one flooding pattern, which is similar to the one encountered in the 1 and 3 atm pressures of the oxygen data. The fraction of electrode flooded is smaller for the air data of Fig. 7 than for the oxygen data of Fig. 6. This may be due to the gas flow rate in the cathode flow channels being higher in the cells using air as the oxidant than in the cells using oxygen as the oxidant. The increased gas flow rate results in increased water removal. The figure also shows the same trends with respect to temperature and pressure as Fig. 6. A higher temperature results in a decrease in flooding while an increase in pressure results in an increase in flooding.

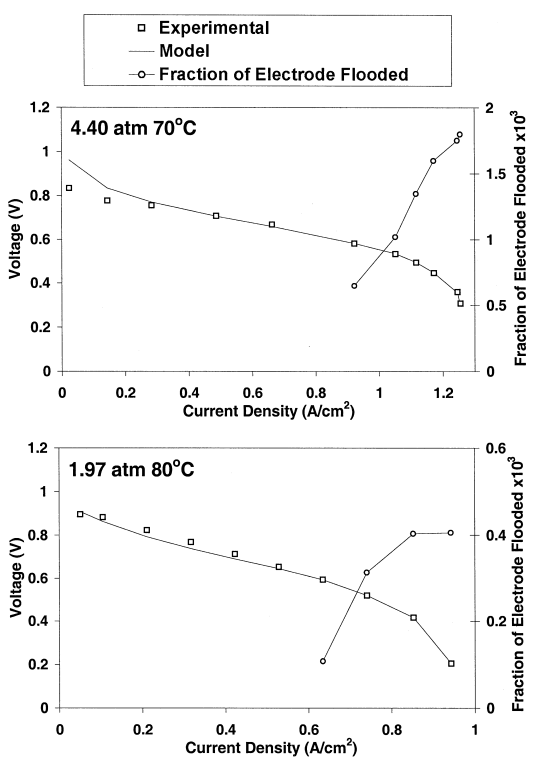

Fig. 8. Modelling the experimental data from Voss et al. [20] (air used as the cathode gas and hydrogen as the anode gas, top graph) and Ledjeff-Hey and Heinzel [21] (oxygen used as the cathode gas and hydrogen and the anode gas, bottom graph) by incorporating different degrees of water flooding in the cathode electrode.

The data from Voss et al. [20] and Ledjeff-Hey and Heinzel [21] were also fitted by the same method as that used for Kim et al. [4] described earlier. The Voss et al. [20] data were from a cell being operated at 4.46 bar (4.4 atm), 70°C and using air as the oxidant. The Ledjeff-Hey and Heinzel [21] data were taken from a cell operating at 2 bar (1.97 atm), 80°C and using oxygen as the oxidant. The cell design parameters used for the fitting of the Voss et al. [20] data are listed in Table 3 while the cell design parameters used for the fitting of the Ledjeff-Hey and Heinzel [21] data are listed in Table 4. The cell performance data from these references were not documented very well and most of the cell design parameters had to be estimated in order to model the data. As a result, the Voss et al. [20] data could not be modelled well at low current densities and the Ledjeff-Hey and Heinzel [21] data could

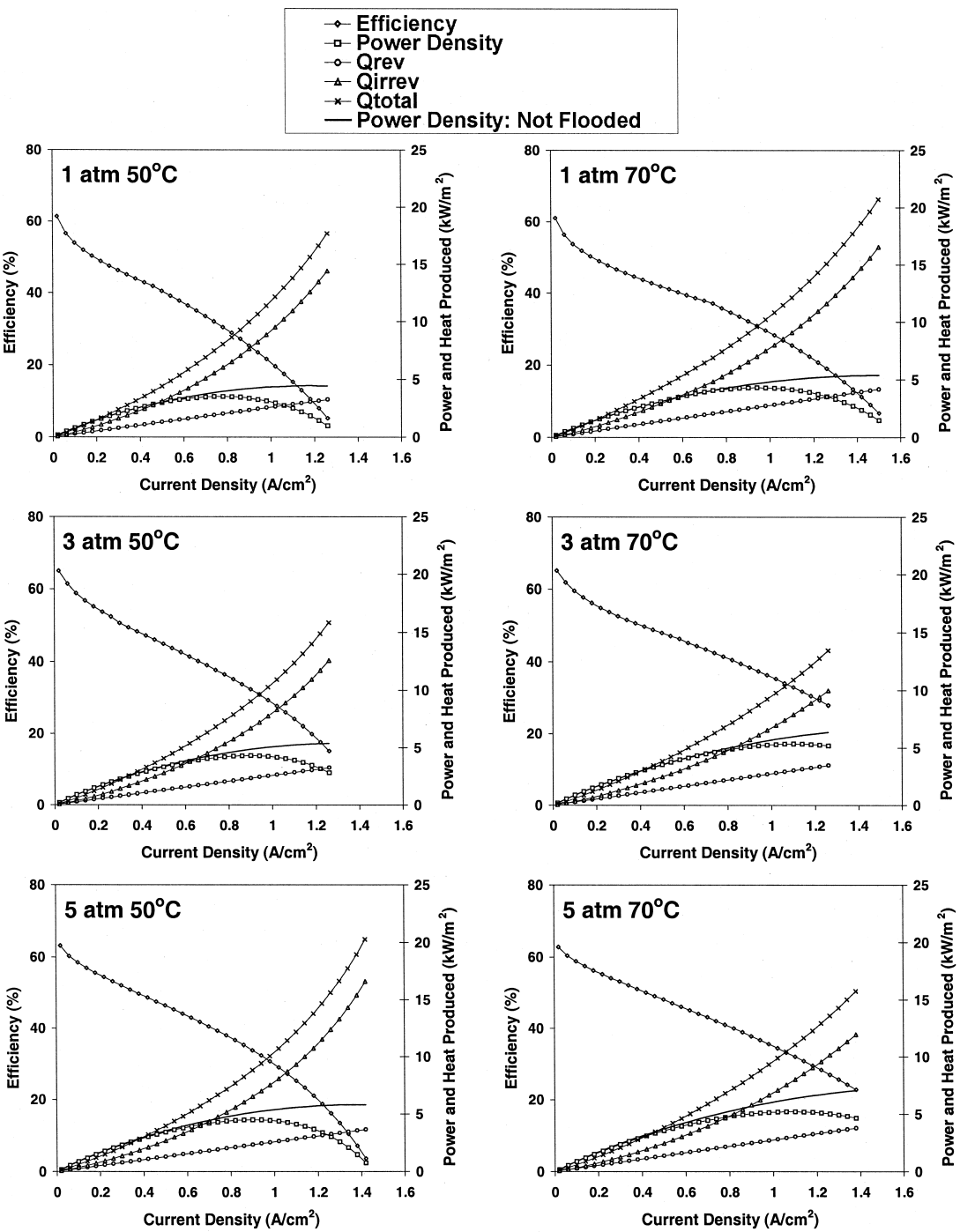

Fig. 9. Cell efficiency, power density, reversible heat produced (Q_{rev}), irreversible heat produced (Q_{irrev}) and total heat produced (Q_{total}) when modelling data from Kim et al. [4]. Oxygen used as the cathode gas and hydrogen as the anode gas.

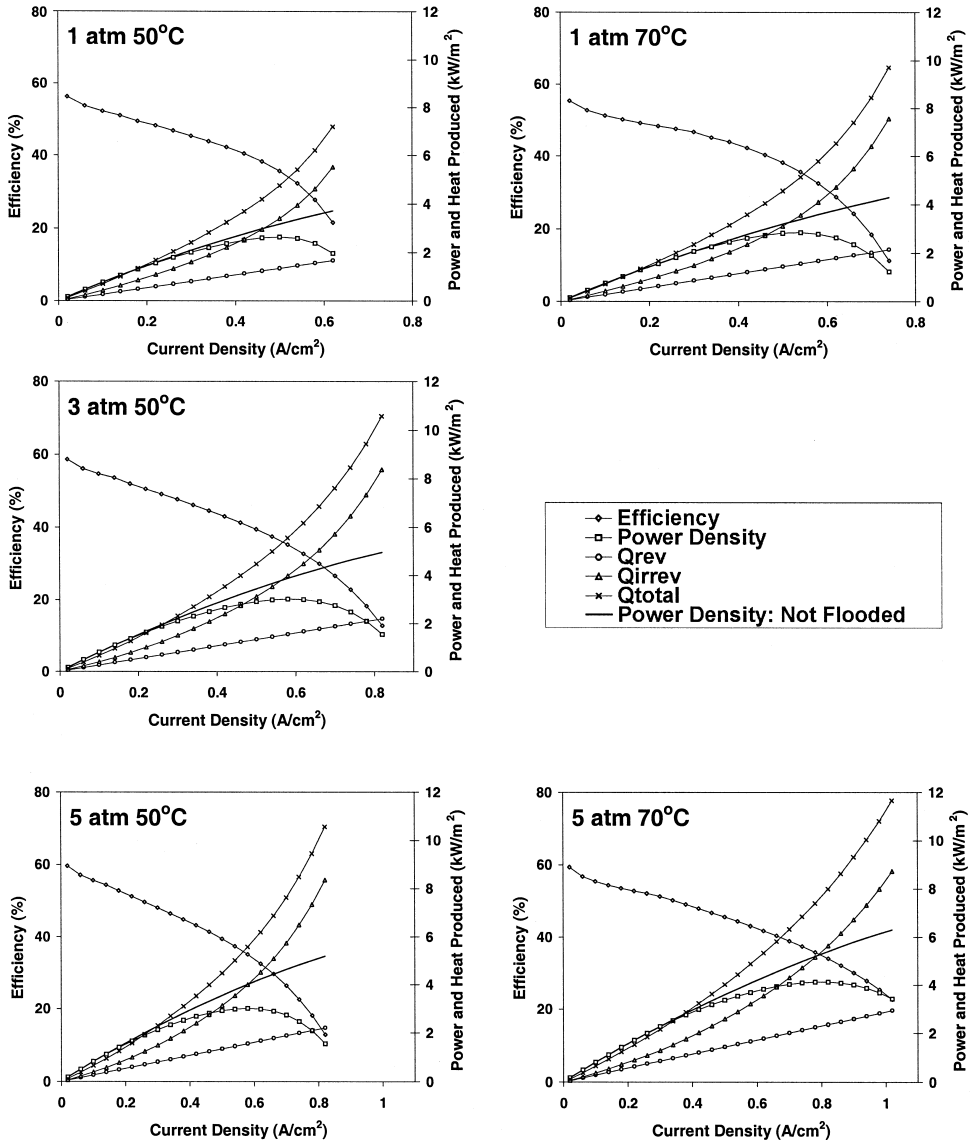

Fig. 10. Cell efficiency, power density, reversible heat produced (Q_{rev}), irreversible heat produced (Q_{irrev}) and total heat produced (Q_{total}) when modelling data from Kim et al. [4]. Air used as the cathode gas and hydrogen as the anode gas.

only be modelled if a stoichiometry value of 1.1 was used for the cathode gas. The result of fitting the model to the data is illustrated in Fig. 8. The resulting flooding schedules resembled that of the low-pressure oxygen data of Kim et al. [4].

The cell efficiency, power density and the reversible, irreversible and total heat produced were also plotted from the model. The cell efficiency is defined as

$$\text{Cell efficiency} = \frac{E}{E_{th}} \tag{66}$$

where E_{th} is the cell thermoneutral voltage and for these calculations it takes on the value of 1.48 V. The power density is calculated by

$$P = EI_{\delta} \tag{67}$$

while the reversible, irreversible and total heat produced are calculated by the following

$$Q_{rev} = (E_{th} - E_r) I_{\delta} \tag{68}$$

$$Q_{irrev} = (E_r - E) I_{\delta} \tag{69}$$

$$Q_{total} = Q_{rev} + Q_{irrev} \tag{70}$$

Fig. 9 illustrates the cell efficiency, power density and the reversible, irreversible and total heat produced when modelling the data with oxygen as the oxidant from Kim et al. [4]. The maximum cell efficiency occurs at a pressure of 3 atm for this data set. Generally, a higher operating pressure results in a higher efficiency, but, because of the flooding

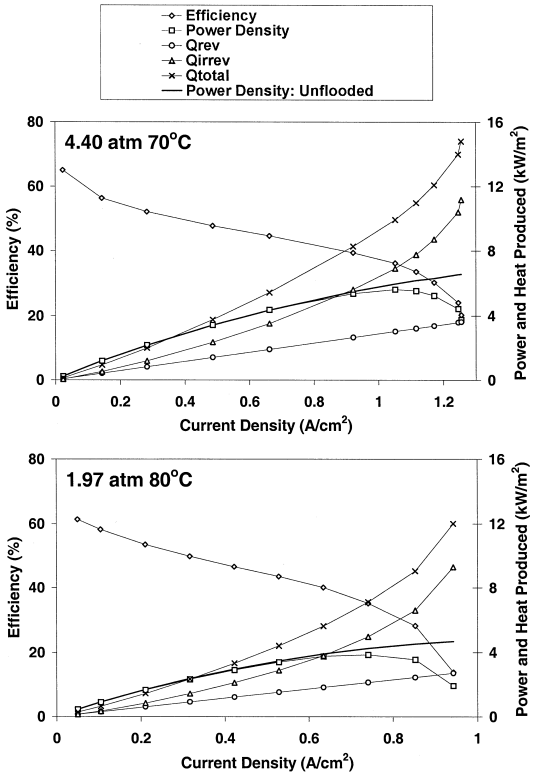

Fig. 11. Cell efficiency, power density, reversible heat produced (Q_{rev}), irreversible heat produced (Q_{irrev}) and total heat produced (Q_{total}) when modelling the data from Voss et al. [20] (air used as the cathode gas and hydrogen as the anode gas, top graph) and Ledjeff-Hey and Heinzel [21] (oxygen used as the cathode gas and hydrogen as the anode gas, bottom graph).

at low current densities at 5 atm, the 3 atm data has a higher efficiency. When flooding is introduced, the power density is reduced substantially and the heat produced increases at a greater rate than when the cell is not flooded. Thus, the performance degradation due to flooding of the cathode electrode backing is apparent. Fig. 10 illustrates the cell efficiency, power density and the reversible, irreversible and total heat produced when modelling the data with air as the oxidant from Kim et al. [4]. Because there was no flooding at low current densities, the highest cell efficiency occurs at a pressure of 5 atm. These data follow the same trends for power density and heat produced as the data in Fig. 9. Fig. 11 illustrates the cell efficiency, power density and the reversible, irreversible and total heat produced when modelling the data from Voss et al. [20] and Ledjeff-Hey and Heinzel [21]. Again, this figure illustrates the power density loss and heat produced when flooding occurs in the cathode electrode backing.

5. Conclusions

A mathematical model of a polymer electrolyte membrane fuel cell has been presented. The essential, fundamental physical and electrochemical processes occurring in the membrane electrolyte, cathode catalyst layer, electrode backing and flow channel has been modelled. A one-dimensional, steady state, isothermal cell with a fully hydrated membrane electrolyte has been assumed. The entire cell polarisation curve was modelled by allowing liquid water to be present in the cathode electrode backing and catalyst layer. This decreased the concentration of oxygen available for reaction and, thus, increased the overpotential of the cathode catalyst layer. It is shown that the present model is in excellent agreement with experimental data when flooding of the electrode is incorporated. The results of applying the flooding model to the experimental data in the literature yields two distinct flooding schedules at high and low cathode gas pressures when pure oxygen is used as the cathode gas. When air is used as the cathode gas, the resulting flooding schedules are all similar for the different pressures and temperatures. The use of air as the cathode gas also reduces the fraction of the electrode flooded due to a higher gas flow rate in the cathode flow channels. It is also observed that increasing the cell pressure increases significantly the extent of water flooding in the electrode and results in the maximum flooding of the cell being reached at a lower current density. Increasing cell temperature results in the onset of flooding occurring at a higher current density. A significant loss of power results from the flooding of the cell.

Acknowledgements

This work was supported by the Natural Sciences and Engineering Research Council of Canada.

References

[1] C.L. Marr, Performance Modelling of a Proton Exchange Membrane Fuel Cell, Masters Thesis, Department of Mechanical Engineering, University of Victoria, Canada, 1996.
[2] C.L. Marr, X. Li, Composition and performance modelling of catalyst layer in a proton exchange membrane fuel cell, J. Power Sources 77 (1999) 17–27.
[3] C.L. Marr, X. Li, An engineering model of proton exchange membrane fuel cell performance, ARI 50 (1998) 190–200.
[4] J. Kim, S. Lee, S. Srinivasan, Modeling of proton exchange membrane fuel cell performance with an empirical equation, J. Electrochem. Soc. 142 (8) (1995) 2670–2674.
[5] J.C. Amphlett, R.M. Baumert, R.E. Mann, B.A. Peppley, P.R. Roberge, Performance modeling of the Ballard Mark IV solid polymer electrolyte fuel cell I: mechanistic model development, J. Electrochem. Soc. 142 (1) (1995) 1–8.
[6] J.C. Amphlett, R.M. Baumert, R.E. Mann, B.A. Peppley, P.R. Roberge, Performance modeling of the ballard mark IV solid polymer electrolyte fuel cell II: empirical model development, J. Electrochem. Soc. 142 (1) (1995) 9–15.
[7] D.M. Bernardi, M.W. Verbrugge, A mathematical model of a gas diffusion electrode bonded to a polymer electrolyte, AIChE J. 37 (9) (1991) 1151–1163.
[8] D.M. Bernardi, M.W. Verbrugge, A mathematical model of a solid polymer electrolyte fuel cell, J. Electrochem. Soc. 139 (9) (1992) 2477–2491.

[9] T.E. Springer, T.A. Zawodzinski, S. Gottesfeld, Polymer electrolyte fuel cell model, J. Electrochem. Soc. 138 (8) (1991) 2334–2342.
[10] T.E. Springer, M.S. Wilson, S. Gottesfeld, Modeling and experimental diagnostics in polymer electrolyte fuel cells, J. Electrochem. Soc. 140 (12) (1993) 3513–3526.
[11] K.R. Weisbrod, S.A. Grot, N.E. Vanderborgh, Through-the-electrode model of a proton exchange membrane fuel cell, Electrochem. Soc. Proc. 23 (1995) 153–167.
[12] T.F. Fuller, J. Newman, Water and thermal management in solid-polymer-electrolyte fuel cells, J. Electrochem. Soc. 140 (5) (1993) 1218–1225.
[13] T.V. Nguyen, R.E. White, A water and heat management model for proton-exchange membrane fuel cells, J. Electrochem. Soc. 140 (8) (1993) 2178–2186.
[14] D. Bevers, M. Wohr, K. Yasuda, K. Oguro, Simulation of a polymer electrolyte fuel cell electrode, J. Appl. Electrochem. 27 (11) (1997) 1254–1264.
[15] M. Eikerling, A.A. Kornyshev, Modelling the performance of the cathode catalyst layer of polymer electrolyte fuel cells, J. Electroanal. Chem. 453 (1/2) (1998) 89–106.
[16] A. Parthasarathy, S. Srinivasan, A.J. Appleby, Temperature dependence of the electrode kinetics of oxygen reduction at the platinum/Nafion interface — a microelectrode investigation, J. Electrochem. Soc. 139 (9) (1992) 2530–2537.
[17] J.S. Newman, Electrochemical Systems, 2nd edn., Prentice-Hall, 1991.
[18] E-TEK, Gas Diffusion Electrodes and Catalyst Materials, 1995 Catalogue, 1995.
[19] Chemical Engineer's Handbook, 5th edn., McGraw-Hill, 1983.
[20] H.H. Voss, D.P. Wilkinson, P.G. Pickup, M.C. Johnson, V. Basura, Anode water removal: a water management and diagnostic technique for solid polymer fuel cells, Electrochem. Acta 40 (3) (1995) 321–328.
[21] K. Ledjeff-Hey, A. Heinzel, Critical issues and future prospects for solid polymer fuel cells, J. Power Sources 61 (1996) 125–127.